Structural determinants of 5-HT$_{2B}$ receptor activation and biased agonism

John D. McCorvy[1,3,6*], Daniel Wacker[1,4,6], Sheng Wang[1,5,6], Bemnat Agegnehu[1], Jing Liu[2], Katherine Lansu[1], Alexandra R. Tribo[1], Reid H. J. Olsen[1], Tao Che[1], Jian Jin[2] and Bryan L. Roth[1*]

Serotonin (5-hydroxytryptamine; 5-HT) receptors modulate a variety of physiological processes ranging from perception, cognition and emotion to vascular and smooth muscle contraction, platelet aggregation, gastrointestinal function and reproduction. Drugs that interact with 5-HT receptors effectively treat diseases as diverse as migraine headaches, depression and obesity. Here we present four structures of a prototypical serotonin receptor—the human 5-HT$_{2B}$ receptor—in complex with chemically and pharmacologically diverse drugs, including methysergide, methylergonovine, lisuride and LY266097. A detailed analysis of these structures complemented by comprehensive interrogation of signaling illuminated key structural determinants essential for activation. Additional structure-guided mutagenesis experiments revealed binding pocket residues that were essential for agonist-mediated biased signaling and β-arrestin2 translocation. Given the importance of 5-HT receptors for a large number of therapeutic indications, insights derived from these studies should accelerate the design of safer and more effective medications.

The human genome encodes 13 distinct 5-HT G-protein-coupled receptors (GPCRs). Drugs targeting 5-HT GPCRs are approved treatments for a diverse array of indications, including obesity, migraine headaches, schizophrenia, anxiety and depression[1,2]. 5-HT receptors also frequently mediate serious drug side effects via unanticipated 'off-target' actions[1,3]. A notable example is the now-banned appetite suppressant fenfluramine, which exerts its potent anti-obesity actions by activating 5-HT$_{2C}$ receptors[4]. Fenfluramine was ultimately withdrawn from the market because of a high incidence of drug-induced valvular heart disease (VHD), which occurs as a result of off-target activation by fenfluramine and its active metabolite norfenfluramine at the closely related 5-HT$_{2B}$ receptor (5-HT$_{2B}$R)[5,6].

Several other medications, including the anti-migraine drugs methysergide and ergotamine[5], the anti-parkinsonian medications pergolide and cabergoline[7], and drugs that treat pituitary adenomas, also have potent off-target actions at 5-HT$_{2B}$R, and they have also been withdrawn or their use severely restricted because of drug-induced VHD[1,5]. Of note, both the VHD and fibrosis associated with carcinoid syndrome have been linked to 5-HT$_{2B}$R activation[8]. Consequently, candidate medications are routinely screened for 5-HT$_{2B}$ agonist activity before progressing to clinical trials[9,10]. Not unexpectedly, 5-HT$_{2B}$ antagonists have been proposed as potential therapeutics for VHD and other fibrotic disorders, including carcinoid syndrome[11]. Thus, understanding the action of drugs at 5-HT$_{2B}$R is clearly important for future drug development.

5-HT$_{2B}$R is a member of the 5-HT$_2$ subfamily of 5-HT receptors, which also includes 5-HT$_{2A}$ and 5-HT$_{2C}$ receptors. 5-HT$_{2B}$R activation via G$_{q/11}$ induces phospholipase C activation, inositol phosphate (IP) accumulation, intracellular calcium release and protein kinase C activation[1,2]. 5-HT$_{2B}$R also recruits β-arrestin2 (also known as arrestin-3; encoded by *ARRB2* in humans) and downstream effector activation[9,12,13]. Drugs such as lysergic acid diethylamide (LSD) and ergotamine (ERG) prefer arrestin recruitment and are considered 'arrestin-biased agonists'[9,12,13].

Over the past few years, there has been an explosion in available GPCR structural information, which has provided a molecular understanding of ligand recognition[14], receptor dynamics and activation[15], and ligand-mediated biased signaling[16]. To date, structures of three 5-HT receptors have been determined by X-ray crystallography, those of the 5-HT$_{1B}$[17,18], 5-HT$_{2B}$[12], and 5-HT$_{2C}$[19] receptors, all in complex with the VHD-inducing anti-migraine drug ERG. For the 5-HT$_{2B}$ receptor, LSD-bound and ERG-bound structures are available and reveal that ergot ligands engage a presumed orthosteric binding pocket (OBP), which is likely shared with the endogenous ligand 5-HT[12,13,17]. Indeed, ERG and LSD engage regions outside this OBP, which we have termed the extended binding pocket (EBP). The OBP of 5-HT receptors shares certain features with the OBP exemplified by the β$_2$-adrenergic receptor (β$_2$AR)[20,21], and it includes highly conserved and critical ligand contacts between the amine nitrogen of the ligands and a highly conserved aspartate in transmembrane domain 3 (TM3; for example, Asp$^{3.32}$ in the Ballesteros–Weinstein numbering scheme[22]), as well as polar and aromatic contacts in TM5 and TM6, respectively. These interactions are thought to facilitate the stabilization of active[23] and G-protein-bound[24] conformational states.

Little is known, however, regarding the 5-HT receptor EBP, which encompasses extracellular portions of TM3 and TM7 and has been

[1]National Institute of Mental Health Psychoactive Drug Screening Program, Department of Pharmacology and Division of Chemical Biology and Medicinal Chemistry, University of North Carolina Chapel Hill Medical School, Chapel Hill, NC, USA. [2]Center for Chemical Biology and Drug Discovery, Department of Pharmacological Sciences and Department of Oncological Sciences, Tisch Cancer Institute, Icahn School of Medicine at Mount Sinai, New York, NY, USA. [3]Present address: Department of Cell Biology, Neurobiology and Anatomy, Medical College of Wisconsin, Milwaukee, WI, USA. [4]Present address: Department of Pharmacological Sciences and Department of Neuroscience, Icahn School of Medicine at Mount Sinai, New York, NY, USA. [5]Present address: State Key Laboratory of Molecular Biology, Institute of Biochemistry and Cell Biology, Shanghai Institutes for Biological Sciences, Chinese Academy of Sciences, Shanghai, China. [6]These authors contributed equally: John D. McCorvy, Daniel Wacker, Sheng Wang. *e-mail: jmccorvy@mcw.edu; bryan_roth@med.unc.edu

proposed as a potential structural feature that may facilitate biased signaling[2]. Support for this hypothesis comes from analysis of the structure of LSD bound to 5-HT_{2B}R, in which LSD stereo-selectively engages TM3 and TM7 to evoke potent β-arrestin2 recruitment[13]. Additional insights into the mechanisms of biased agonism have recently emerged, revealing a key ligand interaction between LSD and Leu209 in extracellular loop 2 (EL2), which increases ligand residence time at the receptor that contributes to enhanced time-dependent β-arrestin2 recruitment[13]. Additionally, both TM5 and the EL2 regions have recently been exploited for biased ligand design at aminergic GPCRs[25]; it is unclear how biased activation occurs via contact with these regions of the receptor.

A clearer understanding of how ligand interactions with key binding pocket residues lead to the stabilization of active or inactive states will facilitate the design of agonist, biased agonist and antagonist drugs. The available structures are with a single ligand type (either agonist or antagonist). In instances where agonist and antagonist structures are available, the ligand chemotypes are structurally diverse (for example, β_2AR, adenosine 2A, the μ and κ opioid receptors, and others[16,26]). Such limitations make it difficult to leverage existing GPCR structural information for structure-guided drug design.

Here we identified key residues responsible for 5-HT_{2B}R activation by comparing the binding modes of chemically similar agonists and antagonists at 5-HT_{2B}R. Notably, we were able to compare the binding mode of methylergonovine with that of its parent anti-migraine drug, methysergide, which differs by a single methyl substituent. To illuminate antagonism, we compared the binding mode of the antagonist lisuride to that of the agonist LSD, which differs by only stereochemistry and an additional nitrogen atom. Finally, we elucidate biased signaling and subtype selectivity by clarifying the binding mode of the selective 5-HT_{2B}R antagonist LY266097. These insights should accelerate the design of safer and more effective medications.

Results

Structural insights into a 5-HT_{2B} activation mechanism. Methysergide is rapidly N-demethylated in vivo to methylergonovine, which is the major active metabolite that mediates methysergide's anti-migraine actions in vivo[27]. Unlike methysergide, which is a 5-HT_{2B}R antagonist, methylergonovine is a potent 5-HT_{2B}R agonist[6] responsible for methysergide-induced VHD[5]. Because methysergide differs from methylergonovine by a single '–CH_3' moiety (Fig. 1a), the pair represents a key ligand set to gain insight into the ligand-based structural features responsible for 5-HT_{2B}R efficacy. Other unsubstituted *N*(1)-H ligands, such as methylergonovine, LSD and ERG, are G_q partial agonists (Fig. 1b). By contrast, the *N*(1)-methyl or alkyl ergoline ligands methysergide (Fig. 1b) and LY215840 (Supplementary Fig. 1a) are 5-HT_{2B}R antagonists.

To identify residues critical for methylergonovine's agonism, we obtained the crystal structure of the 5-HT_{2B}R–methylergonovine complex at a resolution of 2.9 Å (Fig. 1c and Table 1). Methylergonovine forms a salt bridge with $Asp135^{3.32}$ in the presumed orthosteric site, and the ergoline ring system forms an edge-to-face π-π stack with residues $Phe340^{6.51}$ and $Phe341^{6.52}$ in TM6—interactions that are commonly observed in aminergic[20,23] and 5-HT[13,17,19] structures. The binding mode of methylergonovine, when compared with those of LSD and ergotamine, bound to 5-HT_{2B}R revealed a subtly different positioning of the indole *N*(1)-H toward TM5 residues, with ERG being the deepest toward $Ala225^{5.46}$ and LSD being the shallowest toward the backbone of $Gly221^{5.42}$ (Supplementary Fig. 1b). This differential positioning is likely caused by a rotation around the axis of the ionic interaction between Asp3.32 and the protonated ergoline amine group[13]. Similar to ERG, *N*(1)-H of methylergonovine points toward residues $Ala225^{5.46}$ and $Thr140^{3.37}$ (Fig. 1d and Supplementary Fig. 1c). Although the density of *N*(1)-H of methylergonovine was not resolved at 2.9-Å resolution, this hydrogen likely resides between residues $Ala225^{5.46}$ and $Thr140^{3.37}$.

To determine whether residues $Thr140^{3.37}$ and $Ala225^{5.46}$ were involved in methylergonovine's agonism, we mutated the sequences encoding residues $Thr140^{3.37}$ and $Ala225^{5.46}$. $Thr140Ala^{3.37}$ and $Thr140Val^{3.37}$ substitutions substantially diminished methylergonovine's agonism (Fig. 1e) and binding affinity (Supplementary Table 1), despite similar surface expression levels relative to the wild-type receptor (Supplementary Fig. 1d). Although there was not an optimal angle for a hydrogen bonding between *N*(1)-H and residue $Thr140^{3.37}$ in the 5-HT_{2B}R–methylergonovine structure (Supplementary Fig. 1e), the close distance suggests that at least an electrostatic interaction (van der Waals, vdW) between residue $Thr140^{3.37}$ and *N*(1)-H may occur during activation. Indeed, 5-HT, which also contains an *N*(1)-H on the indole, displayed weak G_q activity at $Thr140Ala^{3.37}$ and $Thr140Val^{3.37}$ mutants (Supplementary Fig. 1f), indicating that $Thr140^{3.37}$ is essential for receptor activation. To recapitulate a favorable electrostatic interaction, we created $Thr140Ser^{3.37}$ mutant receptor and found that methylergonovine's G_q agonism (Fig. 1e) and binding affinity (Supplementary Table 1) were spared. By contrast, the substitutions $Ala225Ser^{5.46}$ and $Ala225Gly^{5.46}$ did not substantially affect methylergonovine's G_q agonism (Fig. 1f) or binding affinity (Supplementary Table 1), and they spared 5-HT G_q activity (Supplementary Fig. 1g). Thus, methylergonovine's interaction with $Thr140^{3.37}$ is critical for 5-HT_{2B}R activation.

Structure of a 5-HT_{2B}R $Ala225Gly^{5.46}$ mutant designed to be activated by methysergide. We next sought to understand how the *N*(1)-methyl of methysergide causes 5-HT_{2B}R antagonism. We hypothesized that methysergide's *N*(1)-methyl would either lack interaction with $Thr140^{3.37}$ and/or cause a steric clash with $Ala225^{5.46}$. Methysergide failed to demonstrate any measurable G_q agonist activity with a $Thr140Val^{3.37}$ mutant, where it was expected that the valine and *N*(1)-methyl could form additional vdW interactions to lead to activation (Fig. 2a). By contrast, methysergide demonstrated potent G_q partial agonist activity (Fig. 2a and Supplementary Fig. 2a) with the $Ala225Gly^{5.46}$ mutant, which we hypothesized to introduce more bulk tolerance for methysergide's *N*(1)-methyl—a notion consistent with TM5 engagement appearing to be important for G-protein-dependent agonism[25].

To test this hypothesis, we obtained a structure for the 5-HT_{2B}R($Ala225Gly^{5.46}$)–methysergide complex at 3.1-Å resolution (Fig. 2b, Table 1 and Supplementary Fig. 2b,c). Similar to what was seen in the structure of the 5-HT_{2B}R–methylergonvine complex, methysergide made conserved contacts with $Asp135^{3.32}$, $Phe340^{6.51}$ and $Phe341^{6.52}$. Of note, methysergide's *N*(1)-methyl was pointed down into the space at the mutant $Gly225^{5.46}$ residue. As predicted, removal of a methyl substituent from $Ala225^{5.46}$ to form $Gly225^{5.46}$ created 'space' (for example, bulk tolerance) for the methysergide's *N*(1)-methyl at TM5 (Fig. 2c).

To obtain further insights into methysergide's engagement at TM5, we compared the 5-HT_{2B}R($Ala225Gly^{5.46}$)–methysergide structure to that of inactive-state β_2AR bound to the antagonist ICI-118,551[28]. ICI-118,551, like methysergide, also contains a methyl substitution on its core scaffold that appears to sterically 'push' against residue $Ser207^{5.46}$ in TM5. Alignment of both structures revealed a 1–2 Å shift in TM5, in which the extracellular side of TM5 moved closer to methysergide in the 5-HT_{2B}R($Ala225Gly^{5.46}$)–methysergide structure, whereas ICI-118,551 precluded TM5 movement via its methyl substituent in the β_2AR–ICI-118,551 structure (Fig. 2d). Notably, this TM5 shift is also observed in the nanobody-stabilized active state of β_2AR[23]. Alignment of the structure of the β_2AR–ICI-118,551 complex with that of the nanobody-stabilized active state of β_2AR revealed that ICI-118,551 precludes this inward

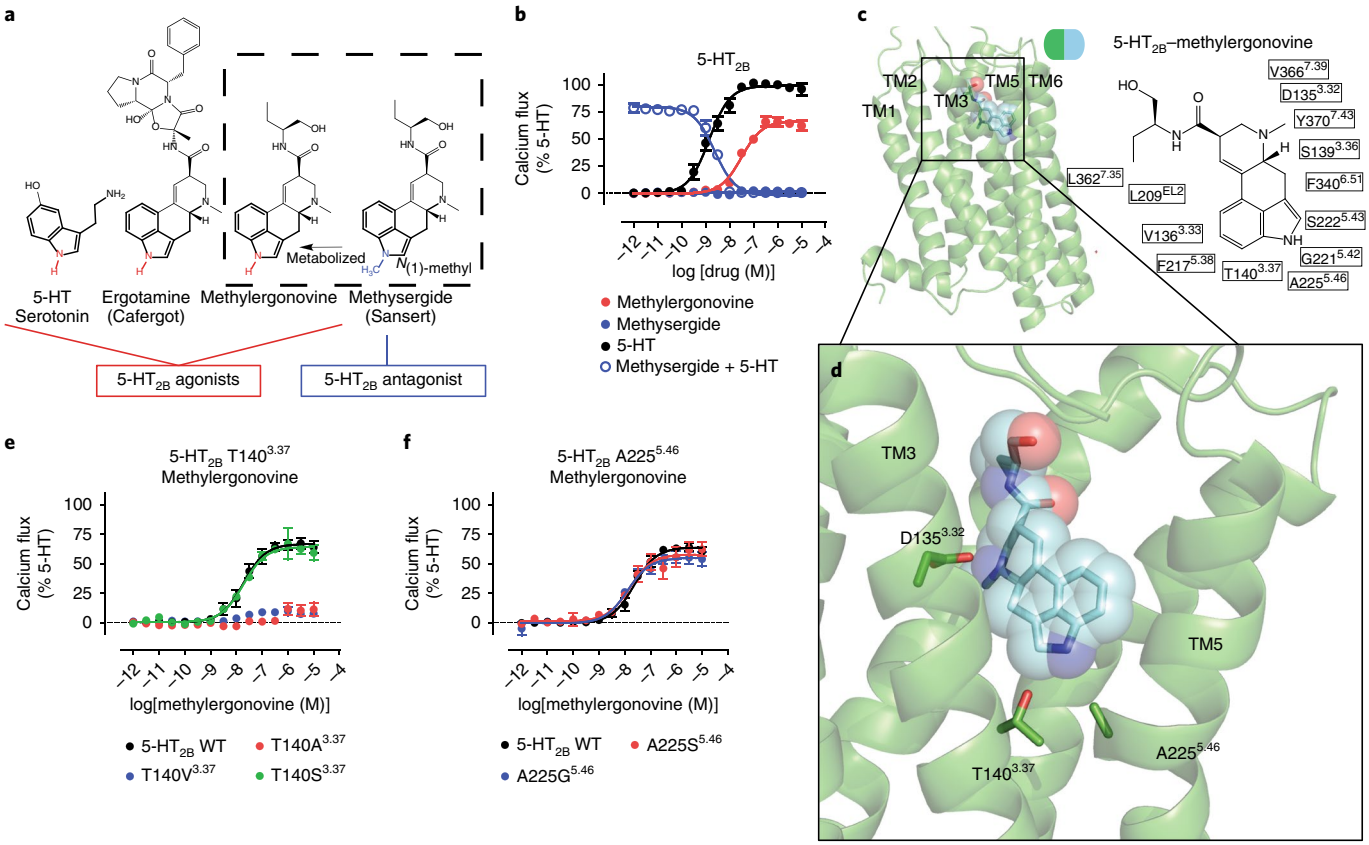

Fig. 1 | Structural insights into a 5-HT$_{2B}$ activation mechanism. a, Structure–activity relationship of 5-HT$_{2B}$R ergoline ligands comparing unsubstituted *N*(1)-H ligands (red) (such as 5-HT, ergotamine and methylergonovine) to *N*(1)-methyl methysergide (blue). **b**, 5-HT$_{2B}$R G_q calcium flux activity by 5-HT (black; EC_{50} = 1.4 nM; E_{max} = 100%) or methylergonovine (red; EC_{50} = 31 nM; E_{max} = 66%) and lack of agonist activity by methysergide (blue, closed circles). Methysergide acts as a competitive antagonist (blue open circles; half-maximal inhibitory concentration (IC_{50}) = 2.4 nM) in response to 5-HT. **c**, Structure of methylergonovine (blue) at 5-HT$_{2B}$R (green) with 2D ligand plots of nearby residues (in single-letter designations) (PDB 6DRY). **d**, Close-up view of the methylergonovine binding pose in the binding pocket highlighting Asp135$^{3.32}$ (D135$^{3.32}$) interacting with the charged nitrogen of methysergide and the indole *N*(1)-H interacting with both Thr140$^{3.37}$ (T140$^{3.37}$) and Ala225$^{5.46}$ (A225$^{5.46}$) in the OBP. **e**, Methylergonovine G_q-mediated calcium flux agonist activity with Thr140Ala$^{3.37}$ (red), Thr140Val$^{3.37}$ (blue) and Thr140Ser$^{3.37}$ (green) mutants (EC_{50} = 18 nM; E_{max} = 64%) relative to wild-type (WT) 5-HT$_{2B}$R (black; EC_{50} = 19 nM; E_{max} = 66%). **f**, Methylergonovine G_q-mediated calcium flux agonist activity in the Ala225Ser$^{5.46}$ (red; EC_{50} = 15 nM; E_{max} = 58%) and Ala225Gly$^{5.46}$ (blue; EC_{50} = 12 nM; E_{max} = 55%) mutants relative to wild-type 5-HT$_{2B}$R (black; EC_{50} = 23 nM; E_{max} = 64%). Data in **b**, **e** and **f** represent the mean ± s.e.m. from *n* = 3 independent experiments, each performed in triplicate. Source data are available online.

TM5 movement via the methyl substituent (Supplementary Fig. 2d). Our results thus reveal that residues Thr140$^{3.37}$ and Ala225$^{5.46}$ are essential for activation.

Structural basis for a 5-HT$_{2B}$ activation mechanism via the extended binding pocket. We next focused on the role of the EBP in receptor activation. We have previously shown that LSD's diethylamide, which is key for LSD's potent hallucinogenic effects[29], contacts TM3 and TM7 within the EBP[13]. Furthermore, we found that recognition of LSD in this region is stereo-selective, as LSD's potent agonism was recapitulated by only the (*S*,*S*)-azetidide stereoisomer, a conformationally restricted diethylamide stereoisomer of LSD[13]. Less clear, however, is the effect of opposing stereochemistry at the C8 position in antagonist versus agonist recognition. Here we sought to examine other ergoline ligands, such as lisuride, which has the same ergoline core scaffold as LSD yet possesses an (*S*)-diethylurea (Fig. 3a) and is a potent 5-HT$_{2B}$R antagonist[30] (Fig. 3b).

To identify the structural basis for lisuride's antagonism, we solved the structure of the 5-HT$_{2B}$R–lisuride complex to a resolution of 3.1 Å (Fig. 3c, Table 1 and Supplementary Fig. 3a,b). Alignment of the 5-HT$_{2B}$R–LSD and 5-HT$_{2B}$R–lisuride structures showed similar binding poses in the OBP, where the indole *N*(1)-H of both LSD and lisuride formed a hydrogen bond with the carbonyl backbone at residue Gly221$^{5.42}$ in TM5 (Supplementary Fig. 3c). Comparison of these poses at the OBP could not entirely explain the difference in pharmacological activity between LSD and lisuride. By contrast, comparison of the EBP poses revealed that the (*S*)-diethylurea of lisuride was exclusively wedged between residues Trp131$^{3.28}$ and Leu132$^{3.29}$ in a hydrophobic stack, making minimal contact with TM7 residues. This resulted in 1.2 Å less contraction of the binding pocket between residues Trp131$^{3.28}$ and Leu362$^{7.35}$ as compared to the distance in the LSD-bound structure. By contrast, LSD's binding pose, in which the diethylamide contacts residue Leu362$^{7.35}$ in TM7 (Fig. 3c), exhibited a more contracted binding pocket. This unexpected difference in binding pose likely explains lisuride's lack of agonism at 5-HT$_{2B}$R, whereas contact with TM7 residue Leu362$^{7.35}$ in the EBP appears essential for LSD's agonism.

To test the hypothesis that ligand contact with TM7 in the EBP facilitates 5-HT$_{2B}$R activation, we made substitutions at residue Leu362$^{7.35}$, which is the closest residue in proximity to lisuride's diethylurea in TM7, to facilitate an interaction between lisuride and TM7. Consistent with our hypothesis, substitution of Leu362$^{7.35}$ with asparagine (Leu362Asn$^{7.35}$), which we predicted would result in formation of a hydrogen bond with the backbone of lisuride's diethylurea moiety, led to G_q partial agonism (half-maximal effective concentration (EC_{50}) = 395 nM, E_{max} = 41%; Fig. 3d). We also

Table 1 | Data collection and refinement statistics

	h5-HT$_{2B}$R-BRIL-2-methylergonovine (PDB 6DRY)[b]	h5-HT$_{2B}$R(Ala225Gly$^{5.46}$)-BRIL-3-methysergide (PDB 6DRZ)[c]	h5-HT$_{2B}$R-BRIL-1-lisuride (PDB 6DRX)[d]	h5-HT$_{2B}$R-BRIL-1-LY266097 (PDB 6DS0)[e]
Data collection				
Space group	$C222_1$	$C222_1$	$C222_1$	$C222_1$
Cell dimensions				
a, *b*, *c* (Å)	59.7, 119.5, 171.0	59.1, 119.3, 172.6	59.4, 118.6, 168.2	59.5, 120.1 169.5
α, β, γ (°)	90, 90, 90	90, 90, 90	90, 90, 90	90, 90, 90
Resolution (Å)	30.0–2.9 (2.99–2.90)[a]	30–3.1 (3.19–3.10)	30.0–3.1 (3.17–3.10)	30.0–3.2 (3.29–3.20)
R_{merge} (%)	15.7 (71.8)	16.3 (84.5)	12.2 (95.0)	15.9 (128.0)
$I/\sigma(I)$	7.7 (1.4)	8.7 (1.2)	10.9 (1.1)	9.8 (1.2)
$CC_{1/2}$	98.0 (56.0)	98.0 (61.2)	99.6 (46.2)	99.4 (39.1)
Completeness (%)	91.8 (81.1)	93.4 (94.4)	97.1 (97.1)	93.5 (96.5)
Redundancy	2.6 (2.1)	3.3 (3.3)	4.4 (4.3)	3.8 (3.8)
Refinement				
Resolution (Å)	2.9	3.1	3.1	3.2
No. reflections	12,436	10,595	10,679	9,725
R_{work}/R_{free}	23.5/27.1	22.5/26.3	24.3/28.6	22.3/26.4
No. atoms				
5-HT$_{2B}$R	2,200	2,174	2,144	2,177
BRIL	733	622	506	637
Ligand	25	26	25	26
Lipid and other	82	79	53	54
B factors				
5-HT$_{2B}$R	72.5	73.8	81.7	82.7
BRIL	87.1	91.1	135.3	146.5
Ligand	70.2	57.7	77.1	81.7
Lipid and other	90.5	84.7	84.6	100.0
R.m.s. deviations				
Bond lengths (Å)	0.003	0.004	0.002	0.002
Bond angles (°)	0.49	0.61	0.76	0.48

[a]Values in parentheses are for the highest-resolution shell. [b]The number of crystals is 11. [c]The number of crystals is 13. [d]The number of crystals is 11. [e]The number of crystals is 8.

substituted Leu362$^{7.35}$ with either phenylalanine (Leu362Phe$^{7.35}$) or tyrosine (Leu362Tyr$^{7.35}$), which could facilitate either a hydrophobic-aromatic interaction (phenylalanine or tyrosine) or a hydrogen bond (tyrosine) with the diethylurea of lisuride. With both mutants, lisuride was a potent partial agonist, with EC_{50} values as low as 77 nM (Fig. 3d) for the Leu362Phe$^{7.35}$ mutant, a potency comparable to that of LSD with wild-type 5-HT$_{2B}$R (EC_{50} = 40 nM, E_{max} = 82%; E_{max} = % maximum efficacy compared with full agonist). Substitution of Leu362$^{7.35}$ with alanine (Leu362Ala$^{7.35}$) impaired LSD's G_q agonist potency by tenfold (EC_{50} = 401 nM, E_{max} = 79%; Fig. 3e), without altering 5-HT$_{2B}$R surface expression levels (Supplementary Fig. 3d). Taken together, our results showing that LSD and lisuride occupy the OBP in a similar fashion yet exhibit different poses in the EBP indicate that ligand engagement with TM7, specifically with Leu362$^{7.35}$, leads to an auxiliary mechanism of agonist activation via the EBP (Fig. 3f).

Divergent actions on β-arrestin recruitment by OBP versus EBP mutations. We previously reported that ergolines, such as ERG and LSD, display a preference for β-arrestin2 recruitment over G_q-mediated calcium flux at 5-HT$_{2B}$R[12] and that LSD's recruitment of β-arrestin2 appears to be time dependent and a product of its slow off-rate from 5-HT$_{2B}$R[13]. A key structural motif identified for LSD's potent β-arrestin2 recruitment is extracellular loop 2 (EL2); however, other regions of the binding pocket that lead to β-arrestin2 recruitment at this receptor remain unexplored. Here we examined the roles of the EBP versus OBP regions for 5-HT$_{2B}$R β-arrestin2 recruitment.

First, we examined the OBP mutants that were critical for G_q activity for methylergonovine and methysergide (at Thr140$^{3.37}$ and Ala225$^{5.46}$, respectively). With the Thr140Ala$^{3.37}$ mutant, methylergonovine failed to recruit β-arrestin2 (Fig. 4a), indicating that the Thr140Ala$^{3.37}$ substitution disrupts both G_q and β-arrestin2 agonism. Similarly, the Ala225Gly$^{5.46}$ substitution, which restores methysergide's G_q agonism, also restored methysergide's β-arrestin2 recruitment (Fig. 4b). These results indicate that OBP activation via Thr140$^{3.37}$ and Ala225$^{5.46}$ leads to equal contributions for G_q activation and β-arrestin2 recruitment, as observed for the endogenous ligand 5-HT (Supplementary Fig. 4a,b).

Unexpectedly, the EBP Leu362Phe$^{7.35}$ substitution, which restored lisuride's G_q agonism, did not restore lisuride's β-arrestin recruitment agonism (Fig. 4c). Although the Leu362Phe$^{7.35}$ substitution did not affect LSD's G_q agonism, it abolished LSD's β-arrestin recruitment (Fig. 4d). Notably, impairment of β-arrestin2 recruitment by substitution at Leu362$^{7.35}$ appeared to be dependent on the type of substitution—Leu362Phe$^{7.35}$ showed the weakest

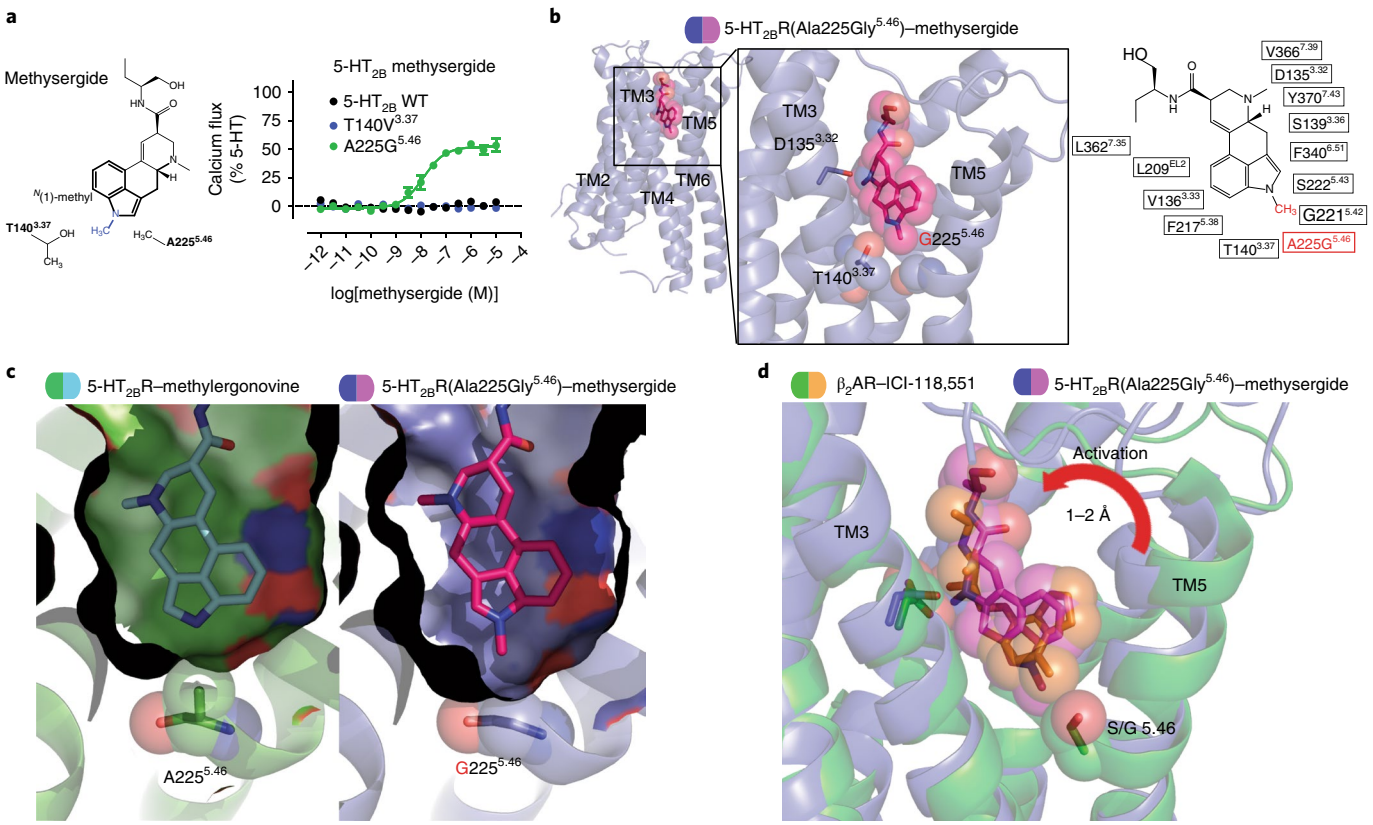

Fig. 2 | Structure of a 5-HT$_{2B}$R(Ala225Gly$^{5.46}$) mutant designed to be activated by methysergide. a, Left, design of the mutation to convert methysergide into an agonist by accommodating the *N*(1)-methyl (blue) with vdW interactions by Thr140Val$^{3.37}$ or with space by Ala225Gly$^{5.46}$. Right, 5-HT$_{2B}$R methysergide G_q-mediated calcium flux activity with wild-type 5-HT$_{2B}$R (black) and the Thr140Val$^{3.37}$ (blue) and Ala225Gly$^{5.46}$ (green) mutants (EC_{50} = 12 nM; E_{max} = 54%). Data represent the mean ± s.e.m. from n = 3 independent experiments, performed in triplicate. Source data are available online. **b**, Structure of the 5-HT$_{2B}$R(Ala225Gly$^{5.46}$) mutant (blue) in complex with methysergide (purple), indicating that *N*(1)-methyl is positioned toward residues Thr140$^{3.37}$ and Ala225$^{5.46}$ in the OBP, which is also illustrated in the 2D ligand plot of nearby residues (PDB 6DRZ). **c**, Space-filling comparison of the 5-HT$_{2B}$R–methylergonovine and the 5-HT$_{2B}$R(Ala225Gly$^{5.46}$)–methysergide structures indicating that the Ala225Gly$^{5.46}$ mutant creates space to accommodate methysergide's *N*(1)-methyl to achieve a similar pose as seen in the 5-HT$_{2B}$R–methylergonovine structure. **d**, Comparison of the binding poses of the 5-HT$_{2B}$R(Ala225Gly$^{5.46}$)–methysergide structure to that of β_2AR (green) in complex with the inverse agonist ICI-118,551 (orange), indicating a 1- to 2-Å shift difference in TM5 commonly observed in active versus inactive structures.

recruitment for β-arrestin with some restoration by Leu362Tyr$^{7.35}$ (Supplementary Fig. 4c).

Further analysis of the Leu362Phe$^{7.35}$ mutant revealed no deficits in G_q function as assessed by PI hydrolysis (Supplementary Fig. 4d) or $G_{q/\gamma 1}$ dissociation, measured by bioluminescence resonance energy transfer (BRET; Supplementary Fig. 4e). By contrast, the Leu362Phe$^{7.35}$ substitution attenuated LSD's time-dependent recruitment of β-arrestin (Supplementary Fig. 4f), as observed previously for the EL2 Leu209Ala substitution[13]. Accordingly, we directly measured LSD's dissociation rate with the Leu362Phe$^{7.35}$ mutant, observing a > 10-fold faster dissociation rate than for wild-type 5-HT$_{2B}$R (Fig. 4e). Thus, the Leu362Phe$^{7.35}$ substitution decreases β-arrestin2 recruitment by accelerating dissociation, thereby contributing to β-arrestin2 recruitment. Taken together, ligand recognition in the OBP results in equivalent G_q and β-arrestin2 activity, whereas ligand recognition in the EBP, specifically at TM7, results in either G_q or β-arrestin2 recruitment activity and divergent effects on ligand bias (Fig. 4f).

Structure of 5-HT$_{2B}$R–LY266097 reveals TM7 as a trigger for biased signaling. Finally, we explored non-ergoline antagonists with distinct scaffolds to determine whether they displayed similar binding modes that were shared with other 5-HT$_{2B}$R antagonists. Although lisuride is a 5-HT$_{2B}$R antagonist, it lacks selectivity for 5-HT$_{2B}$R, as is commonly observed for many ergolines[19]. LY266097, however, is a purported selective 5-HT$_{2B}$R antagonist[31] that contains a distinct tetrahydro-β-carboline pharmacophore, and determining the binding mode of LY266097 could illuminate novel structural determinants of 5-HT$_{2B}$R selectivity.

Accordingly, we crystallized LY266097 in a BRIL-fused 5-HT$_{2B}$R (BRIL; thermostabilized apocytochrome b562RIL) and solved the 5-HT$_{2B}$R–LY266097 structure at 3.2-Å resolution (Fig. 5a, Table 1 and Supplementary Fig. 5a,b). Analysis of LY266097's binding pose revealed that the tetrahydro-β-carboline core scaffold was oriented in the OBP with the charged nitrogen engaging Asp135$^{3.32}$ in TM3 and the tetrahydro-β-carboline core engaging residues Phe340$^{6.51}$ and Phe341$^{6.52}$ in a π-π aromatic stack. Unexpectedly, when we compared the binding modes of LY266097 and lisuride in the EBP, we observed that LY266097's 2-chloro-3,4-dimethoxybenzyl substituent was oriented much closer to TM7 than that of lisuride (Fig. 5b,c). On the basis of our previous finding that TM7 appears to be important for biased agonism, we hypothesized that LY266097 should show preference for either G_q or β-arrestin2 activity. We found LY266097 to be a modest G_q partial agonism without detectable β-arrestin2 activity (Fig. 5d) and confirmed LY266097's G_q partial agonism in an additional assay of G_q function via PI hydrolysis (Supplementary Fig. 5c). We also tested LY266097 in an orthologonal β-arrestin2 recruitment assay using BRET, which measured

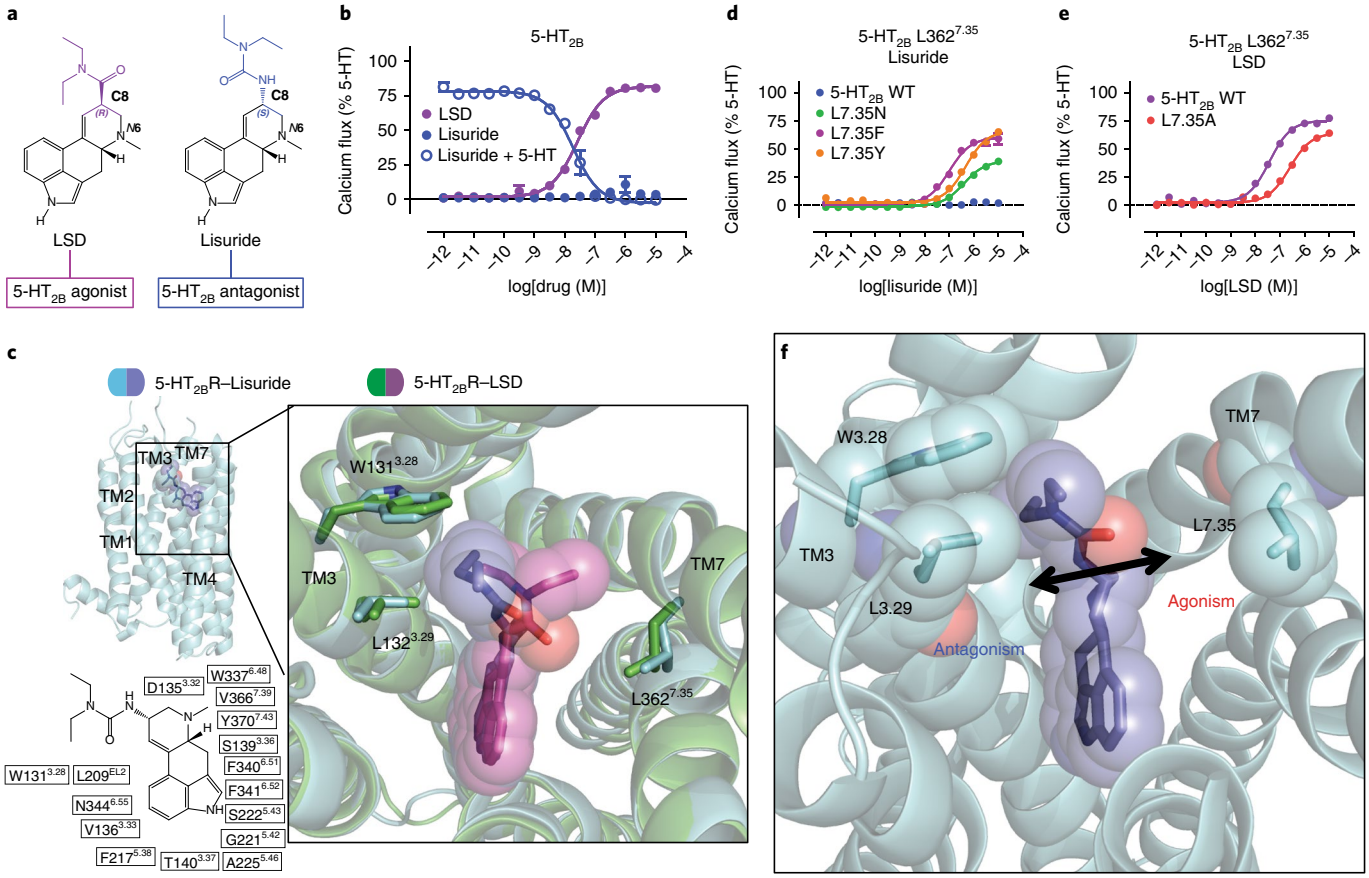

Fig. 3 | Structural basis for a 5-HT$_{2B}$ activation mechanism via the extended binding pocket. a, Comparison of the chemical structures of LSD and lisuride. LSD's (*R*)-diethylamide (purple) and lisuride's (*S*)-diethylurea (blue) lead to 5-HT$_{2B}$R agonism and antagonism, respectively. **b**, 5-HT$_{2B}$R G$_q$-mediated calcium flux activity. LSD shows G$_q$ partial agonist activity (purple; EC$_{50}$ = 40 nM; E_{max} = 82%), whereas lisuride lacks agonist activity (blue, closed circles). Lisuride instead shows competitive antagonism (blue, open circles; IC$_{50}$ = 25 nM). **c**, Structure of lisuride (blue) at 5-HT$_{2B}$R (light blue) in comparison to LSD (purple) bound to 5-HT$_{2B}$R (green), showing lisuride's (*S*)-diethylurea wedged between TM3 residues Trp131$^{3.28}$ and Leu132$^{3.29}$ and making no contact with TM7 Leu362$^{7.35}$ (PDB 6DRX). **d**, Lisuride G$_q$-mediated calcium flux activity for the Leu362Asn$^{7.35}$ (green; EC$_{50}$ = 395 nM; E_{max} = 41%), Leu362Tyr$^{7.35}$ (orange; EC$_{50}$ = 465 nM; E_{max} = 69%) and Leu362Phe$^{7.35}$ (purple; EC$_{50}$ = 77 nM; E_{max} = 60%) mutants. **e**, LSD G$_q$-mediated calcium flux activity for the Leu362Ala$^{7.35}$ mutant (red; EC$_{50}$ = 340 nM; E_{max} = 67%) relative to wild-type 5-HT$_{2B}$R (purple; EC$_{50}$ = 37 nM; E_{max} = 79%). Data in **b**, **d** and **e** represent the mean ± s.e.m. from n = 3 independent experiments, performed in triplicate. Source data are available online. **f**, Schematic illustrating that ligand contact with residue Leu362$^{7.35}$ in TM7 in the EBP leads to 5-HT$_{2B}$R activation.

β-arrestin2 recruitment in real time monitored across specific time points. At no tested time point did LY266097 display β-arrestin2 recruitment (Supplementary Fig. 5d); instead, it displayed potent β-arrestin2 antagonism (Supplementary Fig. 5e). These results indicate that LY266097 has a bias toward G$_q$.

On the basis of our previous results with lisuride and the Leu362Phe$^{7.35}$ mutant, we hypothesized that the extent of G$_q$ agonism by LY266097 is determined by ligand contact between 2-chloro-3,4-dimethoxybenzyl and Leu362$^{7.35}$. To confirm that LY266097's contact with TM7 resulted in selective G$_q$ activation, we tested LY266097 with the Leu362Phe$^{7.35}$ mutant, which was previously found to restore lisuride's G$_q$ agonist activity. As expected, LY266097's G$_q$ agonist activity was abolished with the Leu362Phe$^{7.35}$ mutant (Fig. 5e), suggesting that the bulkiness of the phenylalanine in the Leu362Phe$^{7.35}$ mutant sterically clashed with the 2-chloro-3,4-dimethoxybenzyl moiety, resulting in a lack of agonism. To provide additional evidence that TM7 influences activation via strict steric requirements, we synthesized analogs of LY266097 that lacked either a 2-chloro or a 3,4-dimethoxy substituent on the benzyl moiety, which would be expected to show less TM7 interaction. We found a substituent-dependent decrease in G$_q$-mediated agonist potency, with the unsubstituted benzyl analog showing no detectible G$_q$ agonist activity, indicating that the substitution pattern to LY266097's scaffold conferred G$_q$ agonism (Fig. 5f).

Similar to methysergide, LY266097 contains a methyl substituent on the tetrahydro-β-carboline scaffold that appears to 'push' on TM5 at position Gly221$^{5.42}$ (Fig. 5g), a key residue implicated in conferring 5-HT$_2$ subtype selectivity[19]. To determine whether LY266097's methyl substituent was in part responsible for G$_q$ partial agonism, we synthesized a des-methyl analog of LY266097 and found that it was nearly a full agonist (EC$_{50}$ = 20 nM; E_{max} = 93%; Fig. 5h). These results suggest that the methyl substituent on LY266097 and its interaction with TM5 impair agonism.

Discussion

Here leveraged by four new 5-HT$_{2B}$ crystal structures, including the structure of a mutant receptor (Ala225Gly$^{5.46}$) designed to switch a ligand's efficacy, we provide a comprehensive structural analysis of ligand-specific contacts that lead to GPCR activation. Notably, this study not only identifies mechanisms of 5-HT GPCR activation via the orthosteric site, but also identifies important determinants of β-arrestin recruitment via the EBP, thereby illuminating determinants of ligand bias that could apply to other GPCRs.

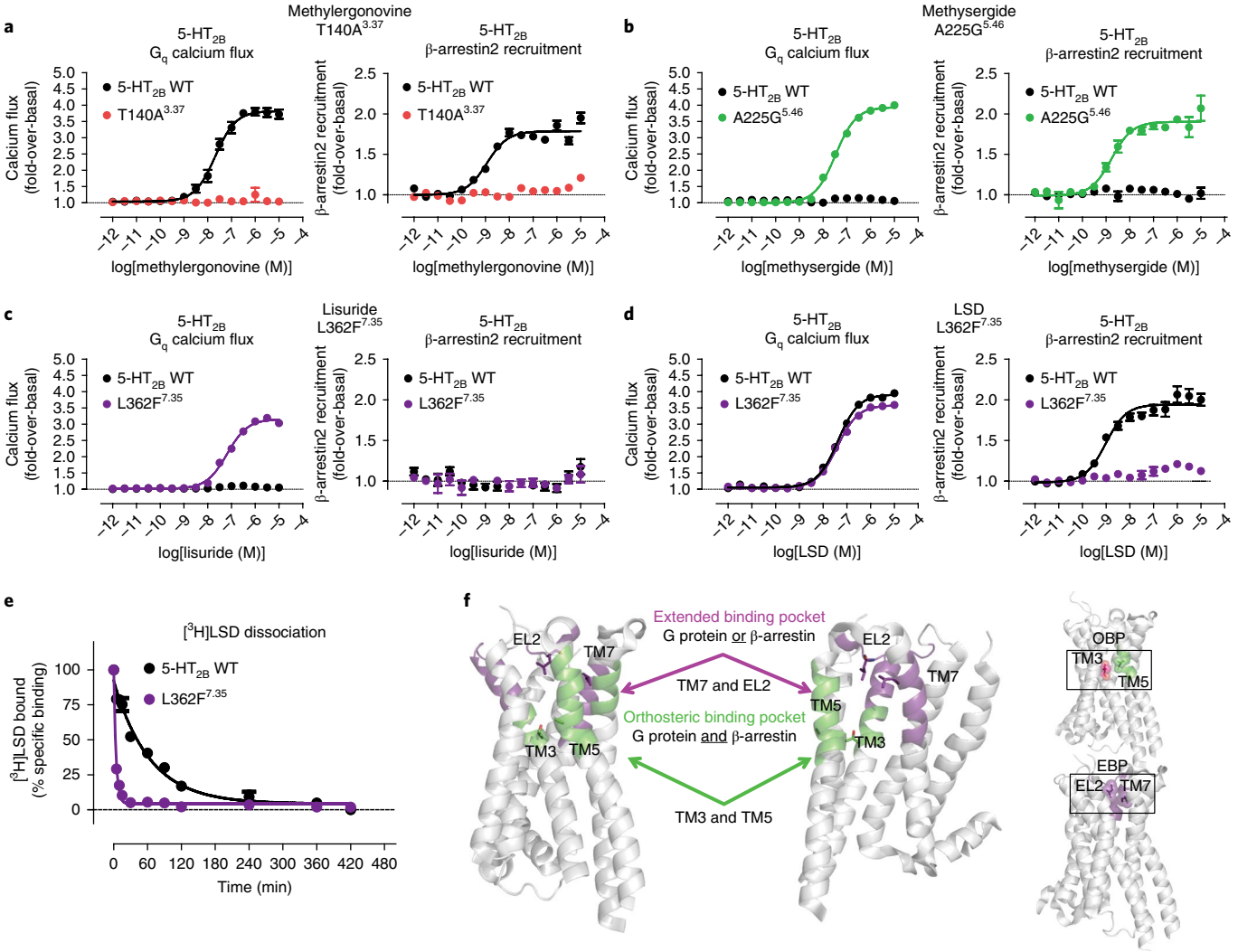

Fig. 4 | Divergent actions on β-arrestin2 recruitment by OBP versus EBP mutations. a, Left, methylergonovine G_q-mediated calcium flux comparing the Thr140Ala$^{3.37}$ mutant (red) to wild-type 5-HT$_{2B}$R (black; EC_{50} = 21 nM). Right, β-arrestin2 recruitment comparing the Thr140Ala$^{3.37}$ mutant (red) to wild-type 5-HT$_{2B}$R (black; EC_{50} = 1.2 nM). **b**, Left, methysergide G_q-mediated calcium flux comparing the Ala225Gly$^{5.46}$ mutant (green; EC_{50} = 33 nM) to wild-type 5-HT$_{2B}$R (black). Right, β-arrestin2 recruitment comparing the Ala225Gly$^{5.46}$ mutant (green; EC_{50} = 1.7 nM) to wild-type 5-HT$_{2B}$R (black). **c**, Left, lisuride G_q-mediated calcium flux comparing the Leu362Phe$^{7.35}$ mutant (purple; EC_{50} = 65 nM) to wild-type 5-HT$_{2B}$R (black). Right, β-arrestin2 recruitment comparing the Leu362Phe$^{7.35}$ mutant (purple) to wild-type 5-HT$_{2B}$R (black). **d**, Left, LSD G_q-mediated calcium flux comparing the Leu362Phe$^{7.35}$ mutant (purple; EC_{50} = 40 nM) to wild-type 5-HT$_{2B}$R (black; EC_{50} = 42 nM). Right, β-arrestin2 recruitment comparing the Leu362Phe$^{7.35}$ mutant (purple) to wild-type 5-HT$_{2B}$R (black; EC_{50} = 0.97 nM). Data in **a**–**d** are expressed as fold change relative to basal levels and represent the mean ± s.e.m. from n = 3 independent experiments, performed in triplicate. **e**, LSD dissociation comparing wild-type 5-HT$_{2B}$R (black; k_{off} = 0.015 min^{-1}) to the Leu362Phe$^{7.35}$ mutant (purple; k_{off} = 0.240 min^{-1}). Data represent the percentage specific binding, indicating the mean ± s.e.m. from n = 3 independent experiments, performed in duplicate. **f**, Schematic comparing the location of the EBP residues Leu209^{EL2} and Leu362$^{7.35}$ (purple), which contribute to either G_q or β-arrestin2 recruitment preference, to the location of OBP residues Thr140$^{3.37}$ and Ala225$^{5.46}$ (green), which have equal contributions to G_q activity and β-arrestin2 recruitment. Source data for the graphs are available online.

Our results with the 5-HT$_{2B}$R–methylergonovine and 5-HT$_{2B}$R(Ala225Gly$^{5.46}$)–methysergide structures illuminate an orthosteric activation mechanism that occurs via ligand engagement with residues Thr140$^{3.37}$ and Ala225$^{5.46}$. Although residue Ala225$^{5.46}$ has been implicated as an important determinant of activation in β-adrenergic receptors[21,32], the role of the highly conserved Thr140$^{3.37}$ residue is less understood. In fact, crystallographic evidence that shows direct ligand engagement with residue Thr140$^{3.37}$ in TM3 is scarce. In rhodopsin, however, the β-ionone ring of retinal, which is critical for receptor activation, is directly engaged with the Glu122$^{3.37}$ residue. Retinal interaction with Glu122$^{3.37}$ has been posited to lead to disruption of a hydrogen bond between Glu122$^{3.37}$ and His211$^{5.46}$, which causes an inward rotation of TM5, transducing disruption of the ionic lock between the intracellular portions of TM3 and TM6[33]. Although here ligand engagement with Thr140$^{3.37}$ appears to involve either a hydrogen bond or an electrostatic interaction, it remains to be seen whether this ligand contact occurs frequently with other ligands or whether its role is more indirect (and in concert with residue Ala225$^{5.46}$) in the activation process, especially considering that residue Thr140$^{3.37}$ is highly conserved across aminergic GPCRs. Our results do emphasize that ligand engagement with residue Ala225$^{5.46}$ and TM5 movement is important for an orthosteric mechanism of class A aminergic GPCRs—both regions highly conserved in aminergic GPCRs that we have previously exploited to design biased ligands[25].

To our knowledge, our results with the 5-HT$_{2B}$R–lisuride structure are the first to reveal a mechanism of activation that occurs

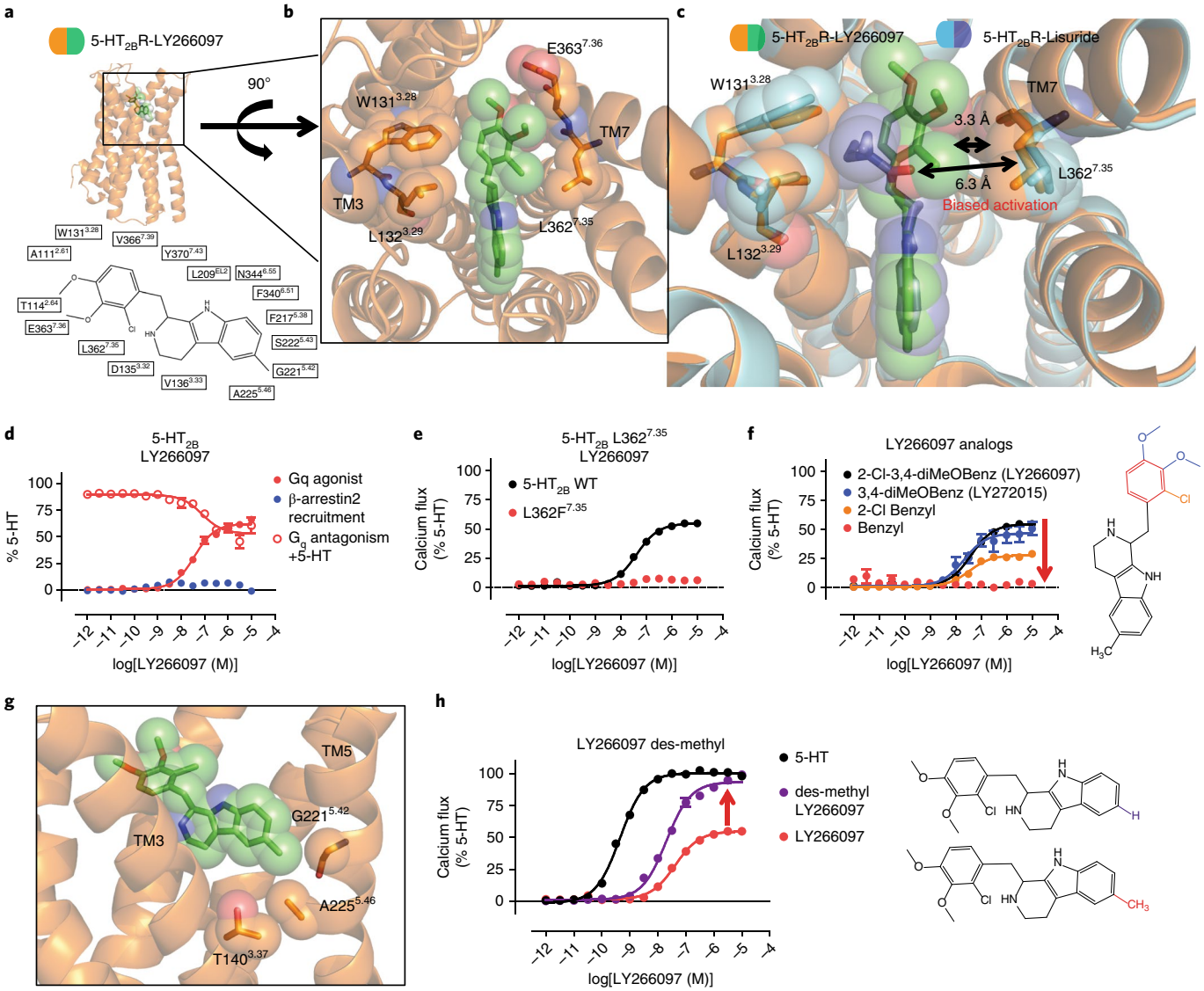

Fig. 5 | Structure of the 5-HT$_{2B}$R-LY266097 complex reveals TM7 as a trigger for biased signaling. Structure of 5-HT$_{2B}$R in complex with LY266097 reveals determinants of ligand bias via TM7. **a**, 5-HT$_{2B}$R (orange) in complex with LY266097 (green) with a 2D ligand plot of nearby residues (PDB 6DS0). **b**, View from the top of the receptor showing that the 2-chloro-3,4-dimethoxybenzyl substituent of LY266097 is oriented in close proximity to residue Leu362$^{7.35}$ in TM7. **c**, Alignment of the 5-HT$_{2B}$R-LY266097 and 5-HT$_{2B}$R-lisuride structures showing that LY266097's 2-chloro-3,4-dimethoxybenzyl substituent is within 3.3 Å of Leu362$^{7.35}$, whereas lisuride's (*S*)-diethylurea is further away, at 6.3 Å from Leu362$^{7.35}$. **d**, Profiling of LY266097 for ligand bias showing G_q partial agonist activity (red closed circles; EC_{50} = 37 nM; E_{max} = 62%) and partial antagonist activity (red open circles; IC_{50} = 78 nM), but no β-arrestin2 recruitment activity (blue). **e**, LY266097 G_q-mediated calcium flux activity comparing the Leu362Phe$^{7.35}$ mutant (red) to wild-type 5-HT$_{2B}$R (black; EC_{50} = 41 nM; E_{max} = 54%). **f**, G_q-mediated calcium flux activity of benzyl-substituted LY266097 analogs 3,4-diMeOBenzyl (blue; EC_{50} = 24 nM; E_{max} = 46%), 2-Clbenzyl (orange; EC_{50} = 35 nM; E_{max} = 28%) and unsubstituted benzyl (red). **g**, 5-HT$_{2B}$R-LY266097 structure showing that the methyl substituent on the tetrahydro-β-carboline scaffold interacts with the 5-HT$_2$-specific residue Gly221$^{5.42}$. **h**, G_q-mediated calcium flux activity of a des-methyl LY266097 analog (purple; EC_{50} = 20 nM; E_{max} = 93%) results in nearly full agonist activity as compared to 5-HT (black; EC_{50} = 0.7 nM) or LY266097 (red; EC_{50} = 41 nM; E_{max} = 54%). Data in **d**–**f** and **h** represent the mean ± s.e.m. from n = 3 independent experiments, performed in triplicate. Source data are available online.

via the EBP, specifically via ligand contact with TM7 at residue Leu362$^{7.35}$. This extended binding region of the receptor is less conserved, allowing for ligand-specific engagement of non-conserved residues, and it likely explains the diverse pharmacological action that results from ligand-specific substituents that project from the core scaffold, as in the case of LSD, where the diethylamide projects away from the core ergoline scaffold. Of note, the same residues, Trp131$^{3.28}$, Leu132$^{3.29}$ and Leu362$^{7.35}$, which are also involved in recognition of LSD's diethylamide and lisuride's diethylurea, compose part of the allosteric site of muscarinic receptors[34]. This suggests that ergoline ligands, such as LSD, access a potential allosteric site, leading to a diverse pharmacological profile (for example, antagonism or biased agonism). However, it remains to be seen whether bona fide allosteric modulators can selectively target the EBP of 5-HT receptors, leading to bias.

Further study of the structural dynamics that lead to activation, either via the OBP or EPB, is needed to clarify trigger motifs (for example, NPxxY, P-I-F, DRY) involved in either balanced or biased activation. Although BRIL-fusion 5-HT$_{2B}$R structures adopt an 'active intermediate' state, more 'active-like' 5-HT$_{2B}$R structures will

likely shed light on key trigger motifs involved in G protein versus β-arrestin2 recruitment. Indeed, current inactive-state structures of 5-HT_{2C}[19] and 5-HT_{1B}[18], which have both been co-crystallized with inverse agonists, implicate the conserved P-I-F trigger as a motif essential for inactivation and biased signaling.

In our study here, Leu362$^{7.35}$ in TM7 appears to be an important determinant of preference for G protein or β-arrestin2 recruitment, as was also implied for κ-opioid receptor biased signaling and for other GPCRs[35,36,37]. In the case of LY266097, which appears to make no specific vdW or hydrogen bond contacts with residues in TM7, our results with Leu362$^{7.35}$ mutants suggest that ligand engagement with TM7 may operate under strict steric constraints, as was similarly observed in the 5-HT_{2B}R Ala225Gly$^{5.46}$–methysergide structure. Notably, hydrophobic contact with Leu362$^{7.35}$, as in the case of LSD, leads to enhanced ligand residence time, and contributions from both TM7 and EL2 serve to stabilize ligand residence time. In fact, increased ligand residence time has been shown to lead to increased β-arrestin2 recruitment over time[13], and it appears to be a hallmark of β-arrestin-biased ligands at aminergic GPCRs[25]. Further study, however, is required to illuminate subsequent signaling after arrestin recruitment, especially as it relates to G protein dependence, as shown in one recent study[8]. Nevertheless, our study illuminates that receptor recognition of small substitutions to core ligand scaffolds directly modulates G protein versus β-arrestin recruitment preferences[37].

Identification of critical residue(s) for 5-HT_{2B}R agonist versus antagonist recognition and encoding of efficacy is important for drug design strategies, which aim to avoid 5-HT_{2B}R activation and VHD. On the basis of our previous structural and functional studies with 5-HT_{2B}R, it is clear that 5-HT_{2B}R represents an attractive receptor template to clarify the structural features necessary for biased signaling as they apply to other class A GPCRs. Insights into the structural basis of agonist versus antagonist action at GPCRs are essential for the design of safer and more effective medications.

Methods

Methods, including statements of data availability and any associated accession codes and references, are available at https://doi.org/10.1038/s41594-018-0116-7.

Received: 21 March 2018; Accepted: 2 July 2018;
Published online: 20 August 2018

References

1. Berger, M., Gray, J. A. & Roth, B. L. The expanded biology of serotonin. *Annu. Rev. Med.* **60**, 355–366 (2009).
2. McCorvy, J. D. & Roth, B. L. Structure and function of serotonin G protein–coupled receptors. *Pharmacol. Ther.* **150**, 129–142 (2015).
3. Allen, J. A. & Roth, B. L. Strategies to discover unexpected targets for drugs active at G protein–coupled receptors. *Annu. Rev. Pharmacol. Toxicol.* **51**, 117–144 (2011).
4. Vickers, S. P., Clifton, P. G., Dourish, C. T. & Tecott, L. H. Reduced satiating effect of d-fenfluramine in serotonin 5-HT_{2C} receptor–mutant mice. *Psychopharmacology* **143**, 309–314 (1999).
5. Roth, B. L. Drugs and valvular heart disease. *N. Engl. J. Med.* **356**, 6–9 (2007).
6. Rothman, R. B. et al. Evidence for possible involvement of 5-HT_{2B} receptors in the cardiac valvulopathy associated with fenfluramine and other serotonergic medications. *Circulation* **102**, 2836–2841 (2000).
7. Zanettini, R. et al. Valvular heart disease and the use of dopamine agonists for Parkinson's disease. *N. Engl. J. Med.* **356**, 39–46 (2007).
8. Gustafsson, B. I., Hauso, O., Drozdov, I., Kidd, M. & Modlin, I. M. Carcinoid heart disease. *Int. J. Cardiol.* **129**, 318–324 (2008).
9. Huang, X. P. et al. Parallel functional activity profiling reveals valvulopathogens are potent 5-hydroxytryptamine$_{2B}$ receptor agonists: implications for drug safety assessment. *Mol. Pharmacol.* **76**, 710–722 (2009).
10. Papoian, T. et al. Regulatory Forum Review*: utility of in vitro secondary pharmacology data to assess risk of drug-induced valvular heart disease in humans: regulatory considerations. *Toxicol. Pathol.* **45**, 381–388 (2017).
11. Hauso, Ø. et al. Long-term serotonin effects in the rat are prevented by terguride. *Regul. Pept.* 143, 39–46 (2007).
12. Wacker, D. et al. Structural features for functional selectivity at serotonin receptors. *Science* **340**, 615–619 (2013).
13. Wacker, D. et al. Crystal structure of an LSD-bound human serotonin receptor. *Cell* **168**, 377–389 (2017).
14. Katritch, V., Cherezov, V. & Stevens, R. C. Diversity and modularity of G protein–coupled receptor structures. *Trends Pharmacol. Sci.* **33**, 17–27 (2012).
15. Latorraca, N. R., Venkatakrishnan, A. J. & Dror, R. O. GPCR dynamics: structures in motion. *Chem. Rev.* **117**, 139–155 (2017).
16. Wacker, D., Stevens, R. C. & Roth, B. L. How ligands illuminate GPCR molecular pharmacology. *Cell* **170**, 414–427 (2017).
17. Wang, C. et al. Structural basis for molecular recognition at serotonin receptors. *Science* **340**, 610–614 (2013).
18. Yin, W. et al. Crystal structure of the human 5-HT_{1B} serotonin receptor bound to an inverse agonist. *Cell Discov.* **4**, 12 (2018).
19. Peng, Y. et al. 5-HT_{2C} receptor structures reveal the structural basis of GPCR polypharmacology. *Cell* **172**, 719–730 (2018).
20. Cherezov, V. et al. High-resolution crystal structure of an engineered human β_2-adrenergic G protein–coupled receptor. *Science* **318**, 1258–1265 (2007).
21. Ring, A. M. et al. Adrenaline-activated structure of β_2-adrenoceptor stabilized by an engineered nanobody. *Nature* **502**, 575–579 (2013).
22. Ballesteros, J. A. & Weinstein, H. Integrated methods for the construction of three-dimensional models and computational probing of structure–function relations in G protein–coupled receptors. in *Methods in Neurosciences* Vol. 25 (ed. Sealfon, S. C.) 366–428 (Academic Press, San Diego, CA, USA, 1995).
23. Rasmussen, S. G. et al. Structure of a nanobody-stabilized active state of the β_2-adrenoceptor. *Nature* **469**, 175–180 (2011).
24. Rasmussen, S. G. et al. Crystal structure of the β_2-adrenergic receptor–G_s protein complex. *Nature* **477**, 549–555 (2011).
25. McCorvy, J. D. et al. Structure-inspired design of β-arrestin-biased ligands for aminergic GPCRs. *Nat. Chem. Biol.* **14**, 126–134 (2018).
26. Stevens, R. C. et al. The GPCR Network: a large-scale collaboration to determine human GPCR structure and function. *Nat. Rev. Drug Discov.* **12**, 25–34 (2013).
27. Bredberg, U., Eyjolfsdottir, G. S., Paalzow, L., Tfelt-Hansen, P. & Tfelt-Hansen, V. Pharmacokinetics of methysergide and its metabolite methylergometrine in man. *Eur. J. Clin. Pharmacol.* **30**, 75–77 (1986).
28. Wacker, D. et al. Conserved binding mode of human β_2-adrenergic receptor inverse agonists and antagonist revealed by X-ray crystallography. *J. Am. Chem. Soc.* **132**, 11443–11445 (2010).
29. Nichols, D. E., Monte, A., Huang, X. & Marona-Lewicka, D. Stereoselective pharmacological effects of lysergic acid amides possessing chirality in the amide substituent. *Behav. Brain Res.* **73**, 117–119 (1996).
30. Hofmann, C. et al. Lisuride, a dopamine receptor agonist with 5-HT_{2B} receptor antagonist properties: absence of cardiac valvulopathy adverse drug reaction reports supports the concept of a crucial role for 5-HT_{2B} receptor agonism in cardiac valvular fibrosis. *Clin. Neuropharmacol.* **29**, 80–86 (2006).
31. Audia, J. E. et al. Potent, selective tetrahydro-β-carboline antagonists of the serotonin 2B (5HT_{2B}) contractile receptor in the rat stomach fundus. *J. Med. Chem.* **39**, 2773–2780 (1996).
32. Sato, T. et al. Pharmacological analysis and structure determination of 7-methylcyanopindolol-bound β_1-adrenergic receptor. *Mol. Pharmacol.* **88**, 1024–1034 (2015).
33. Ahuja, S. & Smith, S. O. Multiple switches in G protein–coupled receptor activation. *Trends Pharmacol. Sci.* **30**, 494–502 (2009).
34. Kruse, A. C. et al. Activation and allosteric modulation of a muscarinic acetylcholine receptor. *Nature* **504**, 101–106 (2013).
35. Nygaard, R. et al. The dynamic process of β_2-adrenergic receptor activation. *Cell* **152**, 532–542 (2013).
36. Staus, D. P. et al. Allosteric nanobodies reveal the dynamic range and diverse mechanisms of G-protein-coupled receptor activation. *Nature* **535**, 448–452 (2016).
37. Che, T. et al. Structure of the nanobody-stabilized active state of the κ opioid receptor. *Cell* **172**, 55–67 (2018).

Acknowledgements

We thank R. Axel (Columbia University) for the HTLA cells expressing TEV-fused β-arrestin2 and R. Fischetti and the staff of APS GM/CA for assistance in the development and use of the minibeam and beam time at GM/CA-CAT beamline 23-ID at the Advanced Photon Source, which is supported by National Cancer Institute grant Y1-CO-1020 and National Institute of General Medical Sciences grant Y1-GM-1104. Use of the Advanced Photon Source was supported by the Office of Science of the US Department of Energy. This work was supported by US National Institutes of Health (NIH) grants R01MH61887 (B.L.R.), R01NS100930 (J.J.), U19MH82441 (J.J. and B.L.R.) and F31-NS093917 (R.H.J.O.), the NIMH Psychoactive Drug Screening Program Contract (B.L.R.) and the Michael Hooker Distinguished Chair of Pharmacology (B.L.R.).

Author contributions

J.D.M. conceived the project, designed the mutant constructs and experiments, performed pharmacological assays, analyzed the data and wrote the manuscript; D.W. expressed

protein, purified the receptor, optimized crystallization conditions, grew crystals for data collection, collected and processed diffraction data, supervised structure determination and assisted with preparing the manuscript; S.W. expressed protein, purified the receptor, optimized crystallization conditions, grew crystals for data collection, collected and processed diffraction data and assisted with preparing the manuscript; B.A. expressed protein, purified receptor, optimized crystallization conditions and grew crystals for data collection; J.L. designed and synthesized LY266097 analogs and performed analytical chemical analysis; K.L. assisted with performing PI hydrolysis signaling studies and analyzed the data; A.R.T. assisted with performing β-arrestin recruitment experiments; R.H.J.O. assisted with performing BRET experiments; T.C. assisted with binding studies; J.J. supervised ligand synthesis and edited the manuscript; B.L.R. was responsible for the overall project strategy and management and edited the manuscript.

Competing interests
The authors declare no competing interests.

Additional information
Supplementary information is available for this paper at https://doi.org/10.1038/s41594-018-0116-7.

Reprints and permissions information is available at www.nature.com/reprints.

Correspondence and requests for materials should be addressed to J.D.M. or B.L.R.

Publisher's note: Springer Nature remains neutral with regard to jurisdictional claims in published maps and institutional affiliations.

Methods

Generation of 5-HT$_{2B}$ receptor constructs. Constructs encoding 5-HT$_{2B}$R for the generation of crystals were based on previously published 5-HT$_{2B}$R constructs in which thermostabilized apocytochrome b_{562} RIL (M7W, H102I, R106L) from *Escherichia coli*—referred to as BRIL—was fused to intracellular loop 3 (ICL3)[38,39] of the receptor[12,13]. The 5-HT$_{2B}$R–LY266097 and 5-HT$_{2B}$R–lisuride complexes were crystallized using a previously crystallized construct (h5-HT$_{2B}$R-BRIL-1) that lacked N-terminal residues 1–35 and C-terminal residues 406–481, contained a thermostabilizing Met144Trp$^{3.41}$ substitution[40] and possessed residues Ala1 to Leu106 of BRIL in place of receptor residues Tyr249 to Val313 of ICL3[38,39]. The 5-HT$_{2B}$R–methylergonovine complex was crystallized by using a different previously crystallized construct[13] (h5-HT$_{2B}$R-BRIL-2) that included Val313 but that was otherwise identical to h5-HT$_{2B}$R-BRIL-1. The 5-HT$_{2B}$R(Ala225Gly$^{5.46}$)–methysergide complex (h5-HT$_{2B}$R-BRIL-3) was generated by QuikChange (Agilent) PCR, mutating the sequence for Ala225$^{5.46}$ to glycine in the h5-HT$_{2B}$R-BRIL-2 construct. All constructs also contained a hemagglutinin (HA) signal sequence followed by a FLAG tag at the N terminus and a PreScission protease site followed by a 10× histidine tag (His tag) at the C terminus to enable purification by immobilized metal affinity chromatography.

Expression and purification of the 5-HT$_{2B}$ constructs. High-titer recombinant baculovirus (>10^9 viral particles/ml) was generated using the Bac-to-Bac Baculovirus Expression System (Invitrogen). Recombinant baculovirus was obtained by transfecting ~5 µg of recombinant bacmid into 5×10^5 settled *Spodoptera frugiperda* (Sf9) cells (Expression Systems) in a 12-well plate (Corning) using 3 µl of Cellfectin II Reagent (Invitrogen). After 5–12 h, medium was exchanged for 1 ml of Sf-900 II SFM medium (Invitrogen), and the plates were incubated for 4–6 d at 27 °C. P0 viral stock was harvested as the supernatant and used to generate high-titer baculovirus stock by infection of 40–1,000 ml of 2×10^6 Sf9 cells/ml and incubation for 3 d. Viral titers were determined by flow cytometry analysis of cells that were stained with phycoerythrin (PE)-conjugated gp64 antibody (Expression Systems)[38]. Expression of 5-HT$_{2B}$R was carried out by infection of Sf9 cells at a cell density of 2×10^6 to 3×10^6 cells/ml in ESF921 medium (Expression Systems) with P1 virus at a multiplicity of infection (MOI) of 3–5. Cells were harvested by centrifugation at 48 h after infection, washed in PBS and stored at −80 °C until use. Cells were disrupted by thawing frozen cell pellets in a hypotonic buffer (10 mM HEPES, 10 mM $MgCl_2$, 20 mM KCl, pH 7.5) containing protease inhibitors (500 µM AEBSF, 1 µM E-64, 1 µM leupeptin, 150 nM aprotinin). Membranes were purified by repeated centrifugation in a high-osmotic buffer (containing 10 mM HEPES, 1 M NaCl, 10 mM $MgCl_2$, 20 mM KCl, pH 7.5) to remove soluble and membrane-associated proteins. Purified membranes were directly flash-frozen in liquid nitrogen and stored at −80 °C until protein purification. Purified membranes were resuspended in a buffer containing 10 mM HEPES, 10 mM $MgCl_2$, 20 mM KCl, 150 mM NaCl (pH 7.5) and protease inhibitors and were incubated for 1 h at room temperature with 50 µM methylergonovine (Sigma, M2776), methysergide (Sigma, M137), lisuride (Tocris, 4052) or LY266097 (Tocris, 4081). After a 30-min incubation in the presence of 2 mg/ml iodoacetamide (Sigma), membranes were solubilized in 10 mM HEPES, 150 mM NaCl, pH 7.5, 1% (wt/vol) n-dodecyl-β-D-maltopyranoside (DDM, Anatrace), 0.2% (wt/vol) cholesteryl hemisuccinate (CHS, Sigma), 25 µM of the indicated complex ligand and protease inhibitors for 2 h at 4 °C. Unsolubilized material was removed by centrifugation at 150,000*g* for 30 min, and 15 mM imidazole was added to the supernatant. Proteins were bound to TALON IMAC resin (Clontech) overnight at 4 °C using approximately 750 µl of resin for protein purified from 2 liters of cells. The resin was then washed with 10 column volumes (CVs) of Wash Buffer I (50 mM HEPES, 800 mM NaCl, pH 7.5, 0.1% (wt/vol) DDM, 0.02% (wt/vol) CHS, 20 mM imidazole, 10% (vol/vol) glycerol and 20 µM of the indicated complexing ligand), followed by 10 CVs of Wash Buffer II (25 mM HEPES, 150 mM NaCl, pH 7.5, 0.05% (wt/vol) DDM, 0.01% (wt/vol) CHS, 10% (vol/vol) glycerol and 20 µM of the indicated complexing ligand). Proteins were eluted in 2.5 CVs of Wash Buffer II + 250 mM imidazole and concentrated in a Vivaspin 20 concentrator with a molecular weight cutoff of 100 kDa (Sartorius Stedim) to 500 µl; imidazole was removed by desalting the protein over PD MiniTrap G-25 columns (GE Healthcare). The C-terminal 10× His tag was removed by addition of His-tagged PreScission protease (GenScript) and incubation overnight at 4 °C. Protease, cleaved His tag and uncleaved protein were removed by passing the suspension through equilibrated TALON IMAC resin (Clontech) and collecting the flow-through. 5-HT$_{2B}$R–ligand complexes were then concentrated to ~30 mg/ml using a Vivaspin 500 centrifuge concentrator with a molecular weight cutoff of 100 kDa (Sartorius Stedim). Protein purity and monodispersity were tested by analytical size-exclusion chromatography.

Lipidic cubic phase crystallization. 5-HT$_{2B}$R–ligand complexes were reconstituted into lipidic cubic phase (LCP) by mixing protein and a monoolein:cholesterol mixture at a ratio of 40%:54%:6% by using the twin-syringe method[5]. Crystallization was done on 96-well glass sandwich plates (Marienfeld) in 50-nl LCP drops that were dispensed from a 10-µl gas-tight pipette (Hamilton) using a handheld dispenser (Art Robbins Instruments) and overlaid with 1 µl of precipitant solution. After optimization, crystals were obtained in 100 mM Tris-HCl pH 8.0, 100 mM sodium formate and 30% (vol/vol) polyethylene glycol 400 (PEG400) for h5-HT$_{2B}$R-BRIL-1–LY266097; 100 mM Tris-HCl pH 7.4–7.7, 30–50 mM ammonium tartrate dibasic and 30% (vol/vol) PEG400 for h5-HT$_{2B}$R-BRIL-1–lisuride; 100 mM Tris-HCl pH 7.2–8.0, 170–190 mM potassium phosphate monobasic and 30% (vol/vol) PEG400 for h5-HT$_{2B}$R-BRIL-2–methylergonovine; and 100 mM Tris-HCl pH 7.3–7.5, 40–100 mM $MgCl_2$ and 30% (vol/vol) PEG400 for h5-HT$_{2B}$R(Ala225Gly$^{5.46}$)-BRIL-3–methysergide. All crystals grew to a maximum size of ~70 µm × 30 µm × 20 µm within 3 d and were harvested directly from the LCP matrix using MiTeGen micromounts before flash-freezing and storage in liquid nitrogen.

Data collection, structure solution and refinement. X-ray data were collected at the 23ID-B and 23ID-D beamline (GM/CA CAT) at the Advanced Photon Source (Argonne, IL, USA), using a 10-µm minibeam at a wavelength of 1.0330 Å and either a MarMosaic 300 charge-coupled detector (CCD) or an Eiger-16m detector (Dectris). Diffraction data were collected by exposing the crystals for 1–3 s to unattenuated beam using primary oscillation. Full datasets for each complex were assembled from several crystals owing to the rapid onset of radiation decay at such high doses. Data were indexed, integrated, scaled and merged using HKL3000[41], and initial phases were obtained by molecular replacement in PHASER[42] using the 5-HT$_{2B}$R coordinates from PDB 4IB4 with the ligand, extracellular loops and orthosteric residues removed. Refinement was performed with PHENIX[43] and REFMAC and included extensive use of simulated annealing to remove model bias. Density was manually examined, and coordinates were rebuilt in COOT[44] using $|2F_o| - |F_c|$, $|F_o| - |F_c|$ and omit maps. After refinement, we did not observe any Ramachandran outliers in any of the structures: 96.34% and 3.66% (5-HT$_{2B}$R–methylergonovine), 95.29% and 4.71% (5-HT$_{2B}$R(Ala225Gly$^{5.46}$)–methysergide), and 96.7% and 3.3% (5-HT$_{2B}$R–lisuride) as well as 97.47% and 2.53% (5-HT$_{2B}$R–LY266097) of residues were in favored and allowed regions, respectively, as defined by Ramachandran statistics. We further observed low Molprobity clash scores of 4.48, 4.94, 3.77 and 3.97 for 5-HT$_{2B}$R–methylergonovine, 5-HT$_{2B}$R(Ala225Gly$^{5.46}$)–methysergide, 5-HT$_{2B}$R–lisuride and 5-HT$_{2B}$R–LY266097, respectively.

G_q-mediated calcium flux FLIPR assays. Stable cell lines were generated for wild-type 5-HT$_{2B}$R and all of the 5-HT$_{2B}$R mutants using the Flp-In 293 T-Rex Tetracycline-inducible system (Invitrogen, mycoplasma-free). Cell lines were maintained in DMEM containing 10% FBS, 10 µg/ml blasticidin (Invivogen) and 100 µg/ml hygromycin B (KSE Scientific). The day before the FLIPR assay, tetracycline-induced cells were seeded into 384-well poly-(L-lysine)-coated black plates at a density of 10,000 cells/well in DMEM containing 1% dialyzed FBS. On the day of the assay, the cells were incubated with Fluo-4 Direct dye (Invitrogen, 20 µl/well) for 1 h at 37 °C, which was reconstituted in drug buffer (20 mM HEPES-buffered Hank's Buffered Salt Solution (HBSS), pH 7.4) containing 2.5 mM probenecid. After dye loading, cells were allowed to equilibrate to room temperature for 15 min and were then placed in a FLIPR^{TETRA} fluorescence imaging plate reader (Molecular Dynamics). Drug dilutions were prepared at 5× final concentration in drug buffer (20 mM HEPES-buffered HBSS, pH 7.4) containing a final concentration of 0.1% BSA and 0.01% ascorbic acid. Drug dilutions were aliquotted into 384-well plastic plates and placed in the FLIPR^{TETRA} for drug stimulation. The drug solutions used for the FLIPR assay were exactly the same as those used for the Tango assay. The FLIPR^{TETRA} was programmed to read baseline fluorescence for 10 s (1 read/s), and afterward 5 µl of drug/well was added and read for a total of 3 min (1 read/s). Fluorescence in each well was normalized to the average of the first ten reads for baseline fluorescence, and then the maximum fold increase was determined and calculated as fold change relative to basal levels (fold-over-basal). Fold-over-basal was plotted as a function of drug concentration, and data were normalized to percent 5-HT stimulation. Data were plotted, and nonlinear regression was performed using 'log(agonist) versus response' in GraphPad Prism 5.0 to yield E_{max} and EC_{50} parameter estimates.

β-arrestin2 recruitment Tango assays. Measurement of β-rrestin2 recruitment at 5-HT$_{2B}$R and its mutants used constructs that contained a TEV protease cleavage site and the tetracycline transactivator (tTA) fused to the C terminus of the receptor. Assays were designed and performed as previously described[45]. HTLA cells expressing TEV-fused β-arrestin2 (derived from HEK cells and kindly provided by R. Axel) were grown and maintained in DMEM containing 10% FBS, 5 µg/ml puromycin and 100 µg/ml hygromycin B. On the day of transfection, medium was removed from the HTLA cells, the cells were washed with PBS, and DMEM containing 10% dialyzed FBS and no antibiotics was added. After at least 1 h, the cells were transfected with the 5-HT$_{2B}$R- or mutant-encoding constructs using a calcium-phosphate precipitation method[46]. After at least 24 h, medium was decanted, and the cells were washed with PBS and detached using trypsin. Cells were collected via centrifugation, resuspended in DMEM containing 1% dialyzed FBS and plated into poly-(L-lysine)-coated 384-well white clear-bottom cell culture plates at a density of 7,000–10,000 cells/well in a total of 40 µl. The cells were incubated at 37 °C and 5% CO_2 for at least 6 h before receiving drug stimulation. Drug solutions were prepared in drug buffer (20 mM HEPES-buffered HBSS, pH 7.4) containing 0.1% BSA and 0.01% ascorbic acid (final concentrations). Drug stimulation was performed using the FLIPR^{TETRA} system by dispensing 10 µl/well.

Drug solutions used for Tango assays, which were performed on the same day, were exactly the same as those used for FLIPR assays. Plates were incubated at 37 °C and 5% CO_2 for at least 20–22 h. Afterward, medium was decanted, plates were blotted to remove excess medium and 20 µl/well of BrightGlo reagent (Promega; diluted 1:20 in drug buffer) was added. The plate was incubated for 20 min at room temperature in the dark before being counted using a Wallac Trilux MicroBeta luminescence counter. Relative luminescence units (RLUs) were plotted as a function of drug concentration, normalized to percent 5-HT, and analyzed using 'log(agonist) versus response' in GraphPad Prism 5.0.

Phosphoinositide hydrolysis assays. PI hydrolysis assays measuring G_q-mediated IP accumulation were performed using a scintillation proximity assay (SPA)[9,47]. On the day before the assay, cells were seeded into 96-well poly-(L-lysine)-coated white plates at a density of 40,000–50,000 cells/well in 200 µl of inositol-free DMEM (Caisson Labs) containing 1 µCi/well (final concentration) [^{3}H]myo-inositol (PerkinElmer) and incubated overnight for 16–18 h at 37 °C and 5% CO_2. The next day, the label medium was siphoned off and replaced with 200 µl of inositol-free DMEM. Drug stimulation was initiated with addition of 50 µl of 5 × concentrated drug dilutions made up in drug buffer (20 mM HEPES-buffered HBSS, pH 7.4) containing 0.1% BSA and 0.01% ascorbic acid (final concentrations). To capture IP accumulation, lithium chloride (10 µl/well; 15 mM final concentration) was added 15 min before lysis. The assay was terminated by decanting the medium and adding 40 µl of 50 mM cold formic acid. After overnight incubation at 4 °C, 10 µl of lysates was added to 96-well flexible, clear microplates (PerkinElmer) containing 75 µl of 0.2 mg/well RNA-binding yttrium silicate beads (PerkinElmer) and incubated for 1–2 h wrapped in foil on a shaker at room temperature. Afterward, plates were centrifuged at 300*g* for 1 min, and radioactivity was measured with a Wallac MicroBeta Trilux plate reader (PerkinElmer) using the SPA paralux setting. IP accumulation data were plotted as counts per minute (CPM) as a function of drug concentration, normalized to percent 5-HT stimulation, and analyzed using 'log(agonist) versus response' in GraphPad Prism 5.0.

Bioluminescence resonance energy transfer arrestin assays. To measure 5-HT_{2B}R-mediated β-arrestin2 recruitment as measured by BRET^1, HEK293T cells (ATCC CRL-11268; 59587035; mycoplasma-free) were co-transfected in a 1:1:15 ratio with constructs encoding human 5-HT_{2B}R with C-terminally fused *Renilla* luciferase (*R*Luc8), GRK2 and N-terminally Venus-tagged β-arrestin2 in DMEM supplemented with 10% dialyzed FBS using TransiT-2020 (Mirus). To measure 5-HT_{2B}R-mediated G_q activation via $G_{q/\gamma 1}$ dissociation, as assessed by BRET^2, HEK293T cells in DMEM supplemented with 10% dialyzed FBS were co-transfected in a 1:1:1:1 ratio with constructs encoding *R*Luc8 fused at residue 121 of human $G_{\alpha q}$ ($G_{\alpha q}$-*R*Luc8), GFP^2 fused to the C terminus of human $G_{\gamma 1}$ ($G_{\gamma 1}$-GFP^2), human $G\beta_1$, and either wild-type 5-HT_{2B}R or a mutant using TransiT-2020. After at least 18–24 h, transfected cells were plated in poly-(L-lysine)-coated 96-well white clear-bottom cell culture plates in DMEM containing 1% dialyzed FBS at a density of 30,000–40,000 cells in 200 µl/well and incubated overnight. The next day, medium was decanted, and cells were washed with 60 µl of drug buffer (1 × HBSS, 20 mM HEPES, 0.1% BSA, 0.01% ascorbic acid, pH 7.4); then, 60 µl of drug buffer was added per well. For kinetic experiments, plates were incubated at 37 °C for at least 20 min before receiving drug stimulation. Afterward, 30 µl of drug (3 ×) was added per well, and the plates were incubated for the designated amounts of time. For β-arrestin2 recruitment assays, 10 µl of the *R*Luc substrate, coelenterazine h (Promega, 5 µM final concentration) was added per well, and the plates were incubated for an additional 15 min to allow for substrate diffusion and immediately read for both luminescence at 485 nm and fluorescent eYFP emission at 530 nm for 1 s/well with a Mithras LB940 instrument. The eYFP/*R*Luc ratio was calculated for each well, and the net BRET^1 ratio was calculated by subtracting the eYFP/*R*Luc ratio for each well from the eYFP/*R*Luc ratio in wells without Venus-β-arrestin2 present. For $G_{q/\gamma 1}$ dissociation assays, 10 µl of the *R*Luc substrate coelenterazine 400a (Nanolight Technology, 5 µM final concentration) was added per well, and the plates were incubated for an additional 10 min to allow for substrate diffusion and then immediately read for both luminescence at 400 nm and fluorescent GFP^2 emission at 510 nm for 1 s/well with a Mithras LB940. BRET^2 ratios were calculated as the ratio of GFP^2 fluorescence to either the net BRET^1 or BRET^2 ratios and were plotted as a function of drug concentration using GraphPad Prism 5. Data were normalized to percent 5-HT stimulation and analyzed using nonlinear regression 'log(agonist) versus response' in GraphPad Prism 5.0.

Radioligand binding assays. Binding assays were performed using stable Flp-In 293 T-Rex tetracycline-inducible cell lines for 5-HT_{2B}R or its mutants. Binding assays were set up in 96-well plates in standard binding buffer (50 mM Tris, 10 mM $MgCl_2$, 0.1 mM EDTA, 0.1% BSA, 0.01% ascorbic acid, pH 7.4) using [^{3}H]LSD (PerkinElmer; specific activity = 76.0–82.2 Ci/mmol) as the radioligand. For competitive binding assays, all assays were performed with various concentrations of cold unlabeled ligands (1 pM to 10 µM), [^{3}H]LSD (0.2–0.7 nM) and resuspended membranes in a total volume of 225 µl. Reactions for competition assays were incubated for 4 h at 37 °C in a humidified incubator until harvesting. For [^{3}H]LSD dissociation assays, assays used at least two or three radioligand concentrations (0.3–2.0 nM), and reactions were pre-incubated for 2 h at 37 °C in a humidified incubator in a total of 200 µl/well. To initiate dissociation, 10 µl of cold excess LSD (10 µM) was added to each well at specific time points ranging from 2 min to 7 h, and immediately at time = 0 min plates were harvested. For all assays, nonspecific activity was defined as the addition of 10 µM SB 206553. Plates were harvested using vacuum filtration onto 0.3% polyethyleneimine-presoaked 96-well Filtermat A (PerkinElmer) and washed three times at 250 µl/well with cold wash buffer (50 mM Tris, pH 7.4). Filters were dried, and scintillation cocktail (Meltilex, PerkinElmer) was melted and allowed to cool to room temperature. Afterward, filter plates were placed in cassettes and read using a Wallac Trilux Microbeta counter (PerkinElmer). Data were analyzed with GraphPad Prism 5.0 using 'One-site-homologous' to yield K_d, 'One-site-Fit Ki' to yield K_i or 'Dissociation-One phase exponential decay' to yield estimates of k_{off}.

Chemistry general procedures. HPLC spectra for all compounds were acquired using an Agilent 1200 series system with a diode array detector. Chromatography was performed on a 2.1 mm × 150 mm Zorbax 300SB-C_{18} 5-µm column with water containing 0.1% formic acid as solvent A and acetonitrile containing 0.1% formic acid as solvent B, at a flow rate of 0.4 ml/min. The gradient program was as follows: 1% B (0–1 min), 1–99% B (1–4 min) and 99% B (4–8 min). High-resolution mass spectra (HRMS) data were acquired in positive-ion mode using an Agilent G1969A API-TOF instrument with an electrospray ionization (ESI) source. NMR spectra were acquired on a Bruker DRX-600 spectrometer (600 MHz ^{1}H, 150 MHz ^{13}C) or a Varian Mercury spectrometer (400 MHz ^{1}H, 100 MHz ^{13}C). Chemical shifts are reported in parts per million (p.p.m.) (δ). Preparative HPLC was performed on an Agilent Prep 1200 series instrument with the UV detector set to 254 nm. Samples were injected into a Phenomenex Luna 75 mm × 30 mm, 5 µm, C_{18} column at room temperature. The flow rate was 40 ml/min. A linear gradient was used with 10% (or 50%) methanol (A) in water (with 0.1% trifluoroacetic acid; TFA) (B) to 100% of methanol (A). HPLC was used to establish the purity of target compounds. All final compounds had > 95% purity using the HPLC methods described above. Synthesis schemes and purification details of the compounds can be found in the Supplementary Note.

Reporting Summary. Further information on research design is available in the Nature Research Reporting Summary linked to this article.

Data availability. Atomic coordinates and structure factors have been deposited in the Worldwide Protein Data Bank (wwPDB) under accession codes 6DRY (5-HT_{2B}R–methylergonovine), 6DRZ (5-HT_{2B}R(Ala225Gly$^{5.46}$)–methysergide), 6DRX (5-HT_{2B}R–lisuride) and 6DS0 (5-HT_{2B}R–LY266097). Generated and analyzed datasets that support the findings of this study are available as source data files or from the corresponding authors upon reasonable request. Source data for Figs 1, 2, 3, 4, 5 are available online.

References

38. Chun, E. et al. Fusion partner toolchest for the stabilization and crystallization of G protein–coupled receptors. *Structure* **20**, 967–976 (2012).
39. Caffrey, M. & Cherezov, V. Crystallizing membrane proteins using lipidic mesophases. *Nat. Protoc.* **4**, 706–731 (2009).
40. Roth, C. B., Hanson, M. A. & Stevens, R. C. Stabilization of the human β_2-adrenergic receptor TM4-TM3-TM5 helix interface by mutagenesis of Glu122$^{3.41}$, a critical residue in GPCR structure. *J. Mol. Biol.* **376**, 1305–1319 (2008).
41. Minor, W., Cymborowski, M., Otwinowski, Z. & Chruszcz, M. HKL-3000: the integration of data reduction and structure solution—from diffraction images to an initial model in minutes. *Acta Crystallogr. D Biol. Crystallogr.* **62**, 859–866 (2006).
42. McCoy, A. J. et al. Phaser crystallographic software. *J. Appl. Crystallogr.* **40**, 658–674 (2007).
43. Adams, P. D. et al. PHENIX: a comprehensive Python-based system for macromolecular structure solution. *Acta Crystallogr. D Biol. Crystallogr.* **66**, 213–221 (2010).
44. Emsley, P., Lohkamp, B., Scott, W. G. & Cowtan, K. Features and development of Coot. *Acta Crystallogr. D Biol. Crystallogr.* **66**, 486–501 (2010).
45. Kroeze, W. K. et al. PRESTO-Tango as an open-source resource for interrogation of the druggable human GPCRome. *Nat. Struct. Mol. Biol.* **22**, 362–369 (2015).
46. Jordan, M., Schallhorn, A. & Wurm, F. M. Transfecting mammalian cells: optimization of critical parameters affecting calcium-phosphate precipitate formation. *Nucleic Acids Res.* **24**, 596–601 (1996).
47. Bourdon, D. M., Wing, M. R., Edwards, E. B., Sondek, J. & Harden, T. K. Quantification of isozyme-specific activation of phospholipase C-β_2 by Rac GTPases and phospholipase-C-ε by Rho GTPases in an intact cell assay system. *Methods Enzymol.* **406**, 489–499 (2006).